Network for Research and Development in Africa
International Journal of Pure and Applied Science Research
ISSN: 2384-5918, Volume 11, Issue 11
PP 162-175 (April, 2024)
DOI: 4572771111120
arcnjournals@gmail.com
https://arcnjournals.org

The Effect of Alkaline Earth Addition on the Structural, Mechanical and Thermophysical Behaviour of Sealing Glasses for SOFCs Applications

L.U. Grema and M.B. Ngawaitu[1]
*[1] Department of Mechanical Engineering, Ramat Polytechnic Maiduguri, Nigeria

Abstract: *A single series of SOFC glass sealants of compositions (15+x)BaO, 15La_2O_3, 5ZnO 5Al_2O_3, 20B_2O_3, and (40-x)SiO_2 with x= 0, 2.5, 5, 7.5, 10 mol% were characterised for their structure property relationship at increasing BaO and decreasing SiO_2 down the series. The presence of BaO as a modifier indicates a dominant role in the glass structure by inducing structural changes. As BaO is added an increase in density, TEC and decrease in T_g as well as hardness and Young's modulus was observed, while indentation fracture toughness fluctuates by exhibiting initial increase followed by a decrease.*

Keywords: *Network Structure, T_g, TEC, SOFC, Mechanical Properties etc.*

1. Introduction

Solid oxide fuel cells (SOFCs) are devices which convert chemical energy into electrical energy through chemical reactions with higher efficiency than conventional thermal energy conversion systems [1, 2]. SOFCs have a self-reformation ability coupled with fuel flexibility [3, 4], such as the use of hydrocarbon and municipal waste [5] and environmentally friendly [6]. These parameters therefore can potentially be an option to help achieve CO_2 reduction targets [7]. SOFCs operate at high temperatures (600-1000^oC) [6, 8, 9], in an oxidizing, reducing and humid environment [10]. The required minimum service life for mobile and stationary applications are 5000 h and 50000 h respectively [11]. Recent reports indicates that more than 75000 h service can be exceeded for stationary applications [12]. There are two popular designs named according to the cell stacking arrangement; planar or tubular [1, 2, 6, 8, 9, 13]. Planar SOFCs are preferred over tubular ones due to a simpler manufacturing process and higher current outputs as planar SOFCs have a shorter current path [10, 13]. The problem with the design of planar SOFCs is that it requires hermetic sealing to function [8, 9] and the hermetic sealing of the electrodes, electrolytes and metallic interconnects remains a key challenge for pSOFCs [14]. Critical sealing positions in a pSOFCs are the inlets and outlets of both anode and cathode to prevent the fuel and oxidants mixing [3, 15]. To generate high voltages cells are stacked in series [16]; a single cell consists of a dense electrolyte, porous anode and cathode made of nickel zirconia cermet and doped lanthanum manganite

perovskite [17]. The commercialization of pSOFCs depends on the reliability of the sealants [1, 2], which must meet a set of requirements such as gas tightness, high temperature stability, chemical stability and compatibility, mechanical integrity, electrical insulation and thermal expansion tailored to match that of other components of the SOFCs [3, 18, 19]. Glass and glass-ceramics are the most commonly used sealing materials because glass based sealants are cheaper and much better than metallic sealants in terms of resistance to dual atmospheres and can be tailored compositionally to meet most of the sealing requirements with glass based sealants also having the advantage of better wetting to sealing interfaces [1, 2, 20]. Seals used in the SOFCs are produced by tape casting or screen printing and can also be applied in form of a paste containing dispersed powder [1, 2].

Two important criteria for the selection of a sealant are the glass transition temperature (T_g) which must be below the operating temperatures of the SOFCs [1, 2, 21], and the thermal expansion coefficient (TEC) which must closely match the TEC of other cell components to avoid thermal stresses due to mismatch [21]. The T_g must not be higher than the operating temperature of the fuel cells as this will subject the other components of the fuel cells to thermal degradation or burnout of substances during sealing and because the glass will not soften below its T_g it is susceptible to cracking as a result of TEC mismatch which is more pronounced below the T_g [17, 22]. Other relevant thermal properties include the glass viscosity during sealing of about 10^6 Pa.s to avoid wicking and the softening temperature T_s [23]. The softening point is viscosity dependent and depicts the flow characteristics of the glass [22]. The viscosity at T_g and T_s are 10^{12} and 10^9 Pa.s respectively and to provide effective hermetic sealing at the operating temperature the viscosity of sealing glasses must be > 10^9 Pa.s [24]. Majority of the glass and glass ceramic compositions are alkali or alkaline earth containing aluminosilicates, borosilicates, borate and phosphate based glasses [25, 26]. Compositions based on alkali silicates are not suitable due to reaction of the alkalis with the SOFC components as they form volatile species (oxides) and also some stable hydroxides and carbonates leading to chromium poisoning [22, 27]. A lot of researchers have focused on aluminosilicate glasses with high barium between 30-35mol% with the well-known consequences of deleterious $BaCrO_4$ formation especially with the chromium containing metallic interconnect and this phase have high TEC compared with other SOFC components and hence leading to seal separation[28]. Glass compositions with boron as the sole network former is prone to weight loss of about 20% in humid environment of the fuel cell and equally reacts with SOFC parts in both oxidizing and reducing conditions [25]. P_2O_5 based glasses also are not suitable for use as sealing glasses due their volatility at the fuel cell operating conditions[26]. Additives in glasses play a specific role for example, both T_g and T_s can be influenced by the presence of alkaline earth oxide in the glass [6]. Alumina controls crystallization in the glass [29]. A small amount of boron oxide B_2O_3, a lower-temperature glass former, reduces the viscosity of glasses, T_g and T_s and improves the wetting ability while SiO_2 is a high temperature network former [29]. La_2O_3 has been used as a viscosity modifier and long-term CTE stabilizer [24]. In addition, BaO reduces T_g, T_s and raises TEC while SrO is a crystallization stimulant and modify T_g, T_s and TEC. ZnO reduces T_g, T_s and sealing temperature, improves flux and reducing agent [13, 24, 29].

In this study, a correlation is drawn systematically in terms of composition structure and properties for barium swapped for silica sealant obtained through melt quench technique. FTIR and Raman spectroscopies are used for the determination of structural changes as a function of composition and correlated with the basic physical properties of the glasses. While XRD and DTA were used for studying phase change and T_g of the glasses.

2. Experimental

2.1 Sample preparation

Glasses were prepared via melt quench technique using (15+x)BaO, La_2O_3(15), ZnO(5) Al_2O_3(5), B_2O_3(20), and (40-x)SiO_2 with x= 0, 2.5, 5, 7.5, 10)(mol%). In making the glass, SiO_2, Al_2O_3, ZnO and La_2O_3 were used as oxides. While boric acid (H_3BO_3) was used as the source for B_2O_3, and $BaCO_3$ for BaO. Batches to produce 300 g of glass were batched using SiO_2 (99.8%) from Glassworks Services), B_2O_3 (99.5%) from Sigma-Aldrich, UK, Al_2O_3(99.5%), BaO (99%), and ZnO(99.8%) from Fisher chemical, UK.
The well mixed batch was transferred to a zirconia stabilized platinum crucible and heated to 1330 °C in an electric furnace for a total of 5 h. After allowing 1 h to achieve a batch free melt a Pt stirrer was inserted into the melt and the melt was stirred during the remaining 4 h of melting during which refining and homogenization occurred. Finally the molten glass was cast into a pre-heated stainless steel mould. After demoulding the still hot glass was transferred to an annealing furnace for removal of thermal stresses during formation, where it was held at 650 °C for 1 h and then cooled to room temperature at a rate of 1 °C/min.

2.2 Sample characterisation

Fourier transforms infrared (FTIR) spectroscopy of glass samples were carried out using Perkin-Elmer instrument via the KBr pellet technique method in the range of 400–4000cm^{-1}. Approximately 2 mg of each sample and 200 mg of KBr was mixed using agate mortar and pressed into pellets of 13 mm diameter using a hydraulic press (Specac®). Spectra in the range 400-4000cm^{-1} were immediately measured. Prior to measurement background scanning was undertaken. Both transmittance and absorbance data were collected after which peaks were assigned different bonds using data in the literature.

Raman spectra were obtained using a Renishaw InVia Raman Spectrometer. Before each test the instrument was calibrated using a Si wafer reference standard. Excitation of the polished and annealed glass surfaces was undertaken using a 514.5 nm laser at a laser power of 20 mW. The laser beam was magnified 50× and focused at a depth just beneath the polished surface. The exposure and acquisition times were both 10 s. The raw data were transferred to wire 3.4 software and a baseline fitted by linearly connecting four points where the spectra goes to zero following the method of Colomban et al.[30]. The deconvolutions of the Raman data were performed with wire 3.4 software and Gaussian fitting using the solver routine in Excel in the region 800-1200cm^{-1} which is the region for the Si-O stretching vibrations. Before fitting the curves to the spectra the data is corrected for temperature and frequency dependent scattering intensities using the Long (1977) correction method [31]. First the background were subtracted by selecting the multiple spline curve option in the wire 3.4 software and the multiplied by Long correction factor (Long 1977) and finally the corrected spectra is normalized. After which the deconvoluted spectra were fitted with Gaussian bands.

Powder X-ray diffraction (XRD) was used to verify if the samples were amorphous or contained some crystalline phases. Both crystalline and glass samples were crushed to fine particles less than 150µm in size and room temperature measurement was carried out using a Siemens D5000 XRD machine with Cu Kα (λ=1.54056Å) radiation. The radiation source was operated at 40 kV and 40 mA. The samples were scanned from 15-70 ^{o} 2θ with a step size of 0.04 at a scan rate of 4.8 s per step.

To evaluate the physical properties, the densities of glass samples were measured using an AccuPyc II 1340 pycnometer gas displacement system. The system uses helium (99.995% pure) as its medium to measure volume of the glass powder by measuring the pressure change of the helium in a calibrated volume.

A DTA curve records thermal reactions of samples on heating or cooling by comparison with an inert reference undergoing identical thermal treatment. DTA and TGA curves were recorded simultaneously in a Perkin Elmer STA8000 using platinum crucible in static air flow. Approximately 40 mg (balance sensitivity 0.2 µg) powders with equivalent weight of alumina as the inert reference were measured from room temperature to 1000 °C (temperature precision ±0.5 ºC) at 10 °C min^{-1}. No cooling curves were acquired for the samples. The glass transition temperature (T_g) was estimated from the onset of first endothermic peak in a DTA curve. For borosilicate glasses this peak appears at 500~600 ºC whereas for aluminosilicate glass it normally is between 700 and 800 ºC. The crystallisation peak, which is exothermic and expected to appear at higher temperature than the glass transition peak, is apparent in all samples studied here, thus an estimation can be obtained of the glass crystallisation temperature (T_p) for all samples.

The thermal expansion coefficients (TEC) were measured using thermo mechanical analyser TMA for all of the glass samples. The samples were sliced into rectangular shapes of size approximately 10×6×6 mm and heated from RT to 650°C at 1°C/min. Samples were re-measured after crystallization of the samples at 800°C for 50 h to assess the effects of any induced crystal phases on the TEC. A typical DTA plot of these glasses is shown in Fig. 1 and displays a glass transition temperature (T_g), two exothermic peaks assigned to be devitrification temperatures (T_p).

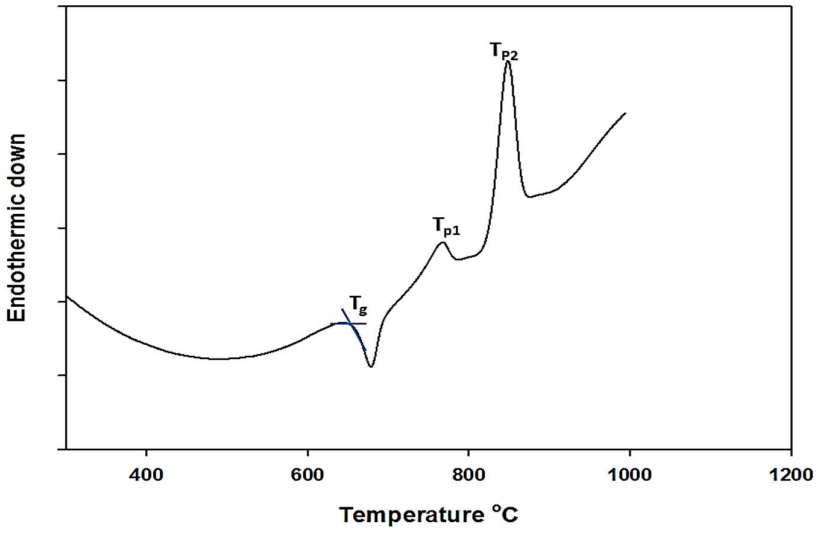

Fig 1 Typical DTA graph for xBa(40-x)Si

3. Results and discussion

The batch compositions used to make these glasses and their corresponding labels are listed in Table 1. Table 2 resumes the values of T_g, TEC and density for the glass series xBa(40-x)Si. All the samples were casted into rectangular shape, and were transparent and free of bubbles. Phase analysis by XRD suggests that the plots exhibits a broad hump appears for each sample

which is a clear indication of the amorphous/glassy nature of each sample. In xBa(40-x)Si series the network former SiO_2 is partially substituted by network modifier BaO and hence the resulting behaviour in these glasses is a result of the combined effect of the oxides.
For structural investigation, the glass samples were characterized using both FTIR and Raman spectroscopies; the Raman spectra were deconvoluted and analyzed. It was stated by Manara [32] that the structure analysis by Raman indicates two types of network structures in the borosilicate glass: the borate structure consists of BO_3 and BO_4 units and the silicate structure in SiO_4 units. As the content of BaO increased against SiO_2, the connectivity of the glass network decreases possibly due to generation of more non-bridging oxygens in the glasses. In the xBa(40-x)Si series additions of BaO led to depolymerisation of the silicate part of the glass network with an increased polymerisation of the borate part of the glass network (conversion of BO_3 to BO_4) as indicated by both FTIR and Raman (see fig1(a) and (b)) [33]. As BaO is added some additional free oxygen is equally added to the glass structure which help converts BO_3 to BO_4 [34] unlike ZnO which may end up in ZnO_4 tetrahedra competing for charge balance with BO_4 and AlO_4 and thus reducing the effective modifier concentration [33].

Glass code	Glass composition (mol %)					
	BaO	ZnO	La_2O_3	Al_2O_3	SiO_2	B_2O_3
15BaSi40	15	5	15	5	40	20
17.5BaSi37.5	17.5	5	15	5	37.5	20
20BaSi35	20	5	15	5	35	20
22.5BaSi32.5	22.5	5	15	5	32.5	20
25BaSi30	25	5	15	5	30	20

Table 1 glass code and compositions in mol%

glass code	T_g/°C	TEC glass ($\times10^{-6}$°C^{-1})	TEC GC($\times10^{-6}$°C^{-1})	Density g/cm^{-3}
15BaSi40	662	8.9	8.9	4.19
17.5BaSi37.5	655	8.7	8.8	4.26
20BaSi35	653	9.8	9.8	4.34
22.5BaSi32.5	652	10.4	11.5	4.45
25BaSi30	644	10.8	11.2	4.51

Table 2 T_g, TEC and density of xBa(40-x)Si series, the TEC also for glass ceramic

3.1 Structural analysis

3.1.1 xBa(40-x)Si series

The systematic variations in the Raman and FTIR spectra of xBa(40-x)Si glasses with increasing BaO are presented in fig 2(a) and (b). There are about seven visible regions in the Raman spectra and five in the FTIR spectra. The intermediate region 800-1200cm^{-1} from both techniques reveals the depolymerising effect of increasing BaO on the SiOSi stretching vibrations with the peaks being shifted to lower wavenumbers and a shoulder appearing around 870 cm^{-1} assigned to Q^0 in the Raman spectra. This behaviour has been reported for both BaO and CaO substitution (see [35]) and a decrease in the peak intensity of this region can be seen more clearly in the FTIR spectra. Peaks assigned to the B-O stretching motion in BO_3 and BO_4 are located between 1250 to 1600cm^{-1} [32, 36, 37] and can be seen in both

Raman and FTIR and these peaks shifted to lower wavenumbers in the Raman spectra with increase in intensity of the 1200cm^{-1} peak assigned to stretching vibration of BO_4 according to Cetinkaya et al in zinc borate glasses [38] and corresponding decrease of the 1400cm^{-1} peak assigned to stretching of B-O of BO_3 characteristics for BO_3 group as BaO increases. For the Raman spectra the top end of the peaks becomes sharper and increase in intensity as it shifts to lower positions which suggest that BO_4 increases with addition of BaO as reported by [39].

The FTIR peaks intensities follow the same pattern as the Raman ones but the peaks in FTIR moved to slightly higher wavenumbers. The decrease in intensity of the 1400 cm^{-1} peak indicates depolymerisation which means that BO_3 in the borate groups and NBOs in the glass structure are reducing according to [39]. The peaks between 600 and 800 cm^{-1} splits into two weak bands in the Raman spectra only; the first weak band at 648-624 cm^{-1} increased in intensity and shifted to lower wavenumbers with increasing BaO. This might be associated with obstructed bending vibration of ring type metaborates groups or the breathing mode of danburite-like rings [35]. The other weak band at 709 -717 cm^{-1} has been identified in FTIR spectra as symmetric stretches in Si-O-(Si, Al) in aluminosilicates [40] and can also be assigned to B-O or B-O-B bending vibration modes of BO_3 units in borosilicate glasses [15]. This band has moved to higher wavenumbers with increasing BaO but the decrease in intensity suggests that the BO_3 group is decreasing with possible conversion into the danburite like structure $[B_2Si_2O8]^{2-}$ since the peak intensity around 624 cm^{-1} has increased [41]. As also explained by Manara this band around 630 cm^{-1} could be the breathing mode of danburite like ring structure including two tetrahedra of both SiO_4 and BO_4 and charge balanced by Na_2O instead of CaO [32], the presence of medium range order structures such as danburite have been reported for borosilicate glasses using Raman spectroscopy [41]. The peak between 400 and 600 cm^{-1} is also seen in both Raman and FTIR with a decrease in intensity and disappearance in the Raman spectra with increasing BaO while in the FTIR it slightly shifts to higher wavenumbers; similar behaviour has been reported by [39]. In general a decrease in intensity and width of these bands is associated with decrease in the bond angles of the SiOSi linkages which determines the frequency of this bending vibration [42, 43]. The lowest wavenumber peak around 250 cm^{-1} in the Raman spectra may be assigned to the bending mode of ZnO_4, however; according to Cetinkaya et al, the 400 to 550 cm^{-1} band in FTIR has also been assigned to the ZnO_4 tetrahedra in borate glasses [38] which suggests that the presence of ZnO_4 unit is indicated by the data from both techniques.

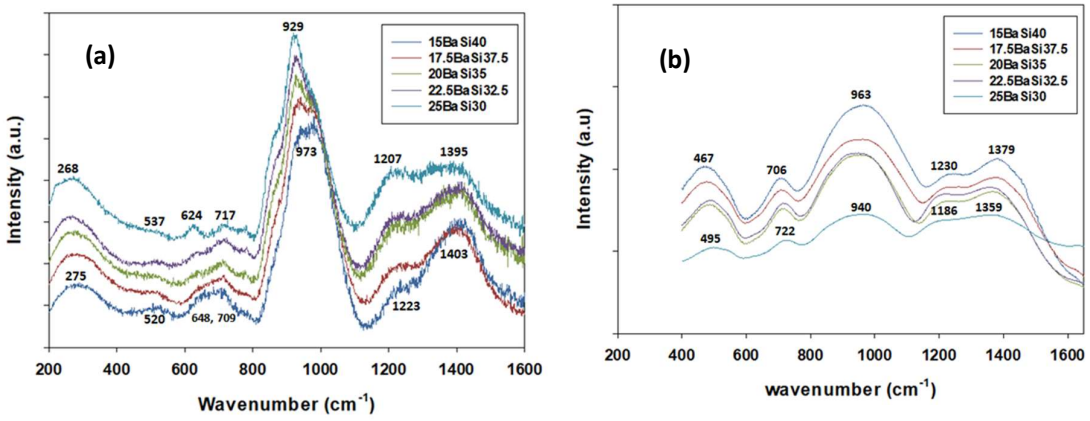

Fig 2 Raman (a) and (b) FTIR spectra for xBa(40-x)Si series

3.2 Thermophysical properties

The glasses are stable up to temperatures above T_g before the emergence of crystallization peaks during the measurement. The glasses have endothermic peaks and exothermic peaks, the onset of the former used to determine the glass transition temperature T_g and the crystallization peak T_c from the later peak. There is a decrease in T_g of about 18 °C from 662 to 644 °C as the BaO increased against SiO_2 in these glasses. There is no significant decrease in the T_g as BaO is increased, a similar behaviour to this is reported in ref [44]. T_g decreases with BaO addition because it creates NBOs in the glass as mentioned in [45]. The decrease in T_g may suggest that the energy needed for structural relaxation of the glass network is also reduced. There are two crystallization peak temperatures in these glasses which may be an indication of phase separation as reported by Lahl et al. [46], or the presence of two different phases in the glass [47]. Usually the TEC of the electrolytes (YSZ, GDC, LSGM) lies between 9.5 to $12\times10^{-6}K^{-1}$ while for the cathode the values 12 to $14\times10^{-6}K^{-1}$, for anode it is 10 to $14\times10^{-6}K^{-1}$ and for the interconnectors it is 11 to $15\times10^{-6}K^{-1}$ [48]. In practice, TECs ranging from $10.0\times10^{-6}K^{-1}$ to $12.0\times10^{-6}K^{-1}$ is considered optimal for SOFC applications, because under this condition, the thermal stress generated is smaller than the strength of the glass, and the cell can work stably at high temperatures [49].

The TECs of all compositions of seal glass are measured from room temperature (RT) to glass transition (T_g) and are presented in fig 3.

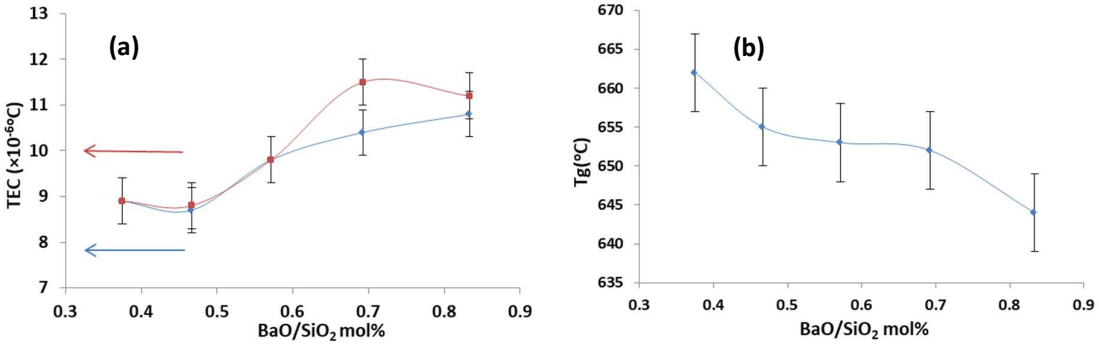

Fig 3 (a) TEC of glass in blue line and glass ceramic in red line, (b) T_g of for xBa(40-x)Si series

The large size of BaO expands the network and weakens the structure leading to decrease in T_g and increase in TEC of the glasses. [50, 51]. There is not much difference between the TEC of the glass and glass ceramics except for BaO/SiO_2 ratio around 0.7 where the TEC for the glass ceramic is higher and at 0.83 slightly higher than that of the glass sample.

3.3 Density and molar volume

The compositional variation of density is shown in fig 4(a). Density increases with increasing BaO in the studied glasses. For all glass compositions, the density increases approximately linearly with the modifier additions. Since SiO_2 were substituted for BaO changes in the average molar mass of the glasses occurs. In the xBa(40-x)Si series an increase in density is evident and the molar volume fluctuates in increase and decrease pattern with BaO additions due to the higher molecular weight of barium 153.3g/mol and high ionic radius of Ba^{2+} (1.49Å) which expands the glass structure and decreases the glass compactness [3, 36, 52]. The observed unusual behaviour where both density and molar volume increase in the same direction have been previously reported for $RO\text{-}Al_2O_3\text{-}B_2O_3$ (RO = Mg>Ca>Sr) containing glasses [53]. The molar volume of xBa(40-x)Si increased and then decreased at a BaO/SiO_2

ratio of 0.57 and then increased again. This type of anomalous drop in molar volume have been reported by Bourgel et al, and is associated with the tendency of the network to densify its structure in barium borosilicate glasses at 25<x<48 mol% of BaO [54].

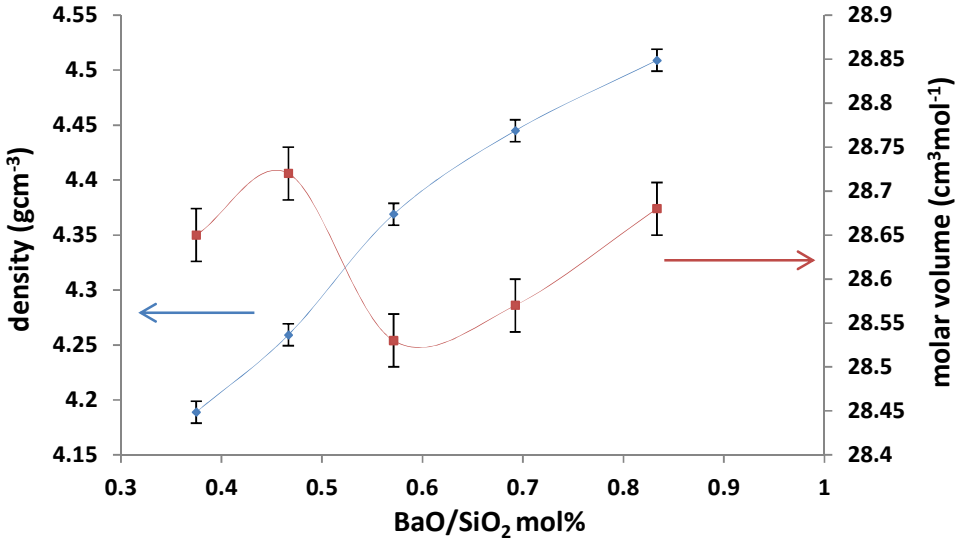

fig 4(a) Density and molar volume

3.4 X-ray Diffraction (XRD)

As indicated earlier the absence of sharp peaks in the as made glass samples suggest that there are no crystalline phases, and the broad hump at low angles around 28° (Bragg angle) indicates amorphous nature, as well as long range structural disorder in these glasses regardless of compositional differences (see fig 5(a) and (b) for xBa(40-x)Si series). After 50h isothermal heat treatment of xBa(40-x)Si series, the XRD pattern indicates that glass (glass ceramic) contains crystalline lanthanum borosilicate phase with PDF card number no (04-010-1343). The intensities of the dominant peaks around 30° seem to decrease with increasing BaO and the peak heights are smallest for 25mol% BaO because decreasing silica removes one major constituent of the phase. As reported by [55] 7 out of 10 phases in the SiO_2-B_2O_3-La_2O_3 ternary contains silica as part of the phases formed; the three phases observed in this study all contained silica. The lanthanum borosilicate single phase shown in fig 5 (b) was also reported by [56] who claimed that it was the first La-borosilicate to be synthesized and its structure solved [56]. Lanthanum and neodymium are reported to be able to form single crystal phase in soda lime borosilicate glasses and the amount of the phase is heat treatment dependent [57].

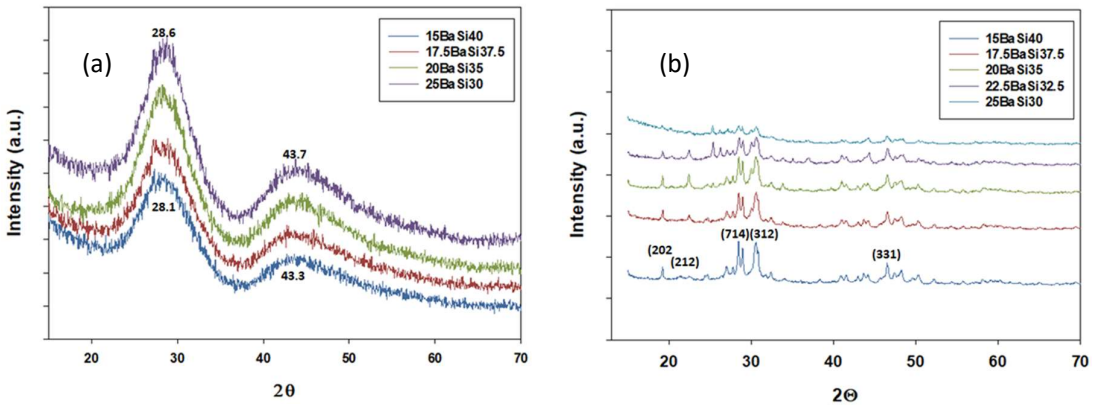

Fig 5 XRD xBa(40-x)Si (a) glass (b) glass ceramic

Glass code	Vicker's Hardness, H_V(GPa)	Young's Modulus E(GPa)	Bulk Modulus K(GPa)	Shear Modulus, G(GPa)	Poisson's Ratio, (v)	Indentation fracture toughness, K_{IC}(MNm$^{-3/2}$)	Glass transition temperature, T_g(°C)
15BaSi40	5.7 ± 0.3	87.3 ± 1.4	75.9 ± 0.51	33.4± 0.24	0.308±0.007	0.77± 0.01	662± 10
17.5BaSi37.5	6 ± 0.7	86.2 ± 1.4	74.8 ± 0.5	33.0± 0.24	0.307±0.007	0.78± 0.02	655± 10
20BaSi35	5.4 ± 0.3	85.7 ± 1.1	74.6 ± 0.55	32.7± 0.15	0.308±0.007	0.80± 0.02	653± 10
22.5BaSi32.5	5.2 ± 0.3	84.6 ± 1	77.3 ± 0.5	32.1± 0.14	0.317±0.007	0.74± 0.01	652± 10
25BaSi30	5.2 ± 0.3	81.2 ± 1	78.5 ± 0.51	30.6± 0.14	0.327±0.007	0.69± 0.01	644± 10

Results III: Mechanical properties

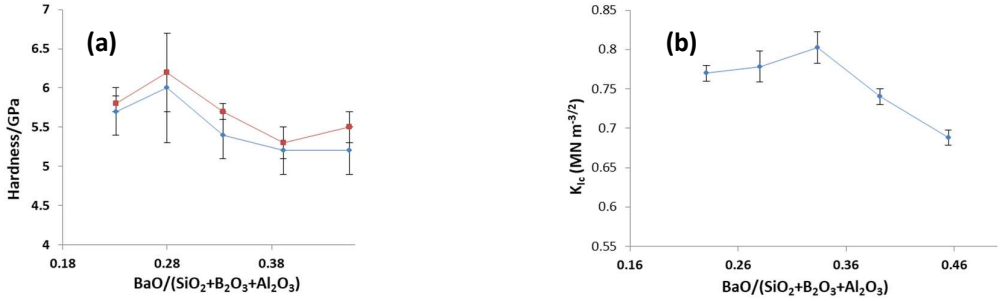

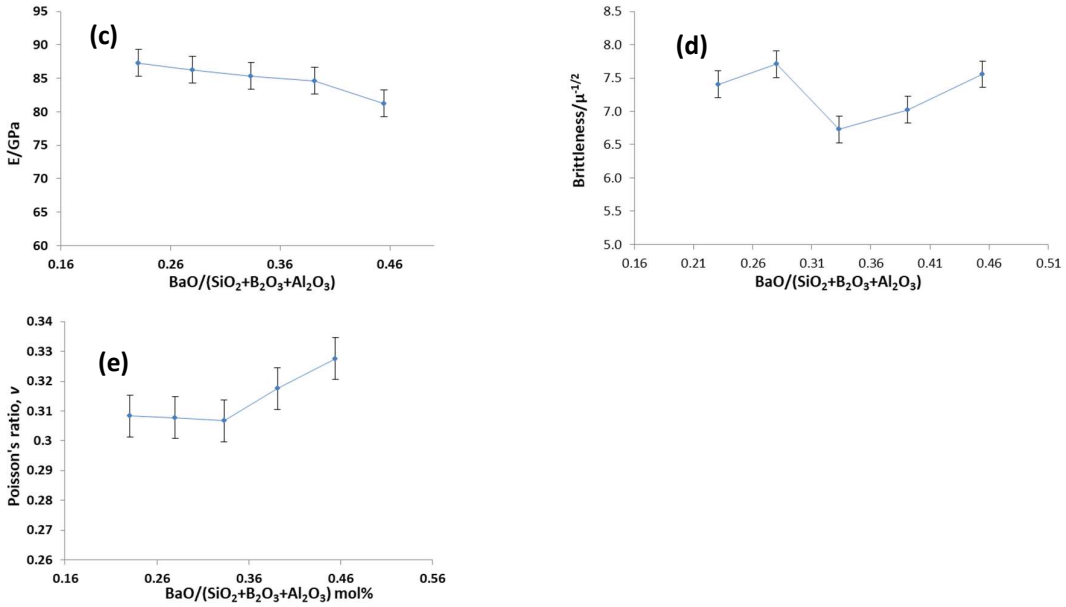

Figure 6: Hardness of glass blue line and glass ceramic red line (a) Indentation fracture toughness (b) Young's modulus (d) Brittleness and (e) Poisson's ratio of xBa(40-x)Si versus BaO/total network formers

The addition of BaO into xBa(40-x)Si leads to a decrease in hardness and Young's modulus as E is linearly proportional to field strength and bond strength of the oxides in the glass, so increasing BaO with lower field strength decreases the E of the glass [45] (fig 6(a) and (c)) while indentation fracture toughness (fig 6(b)) exhibits an initial increase and then decreased at a ratio of BaO/total network formers of ~ 0.3 in these glasses. The hardness is slightly higher for the glass ceramics after crystallization as compared with the parent glasses. The reason for the decrease in hardness and modulus is because BaO, which has a low field strength is less attracted to the network anions and thus is less well bonded into the glass. BaO containing glasses were reported by Hand and Tadjiev to have lower hardness [58]. There is no structural evidence to support the initial rise in indentation fracture toughmess seen in fig 6(b) as the polymerisation index (fig 7) indicates decreases with BaO additions. This would suggest that the behaviour of the indentation fracture toughness is dependent on other factors including energy dissipation process such as plastic deformation, crack branching and blunting occuring at the crack tip and not associated only with energy required to fracture bonds as explain by Yoshida et al, for Vickers indentation of sodium borosilicate glasses [59]. A similar effect on mechanical properties of lanthanum borosilicate glass by all the alkaline earths modifiers depending on their field strength was given in the order ($Mg^{2+} > Ca^{2+} > Sr^{2+} > Ba^{2+}$) was reported by [36] and found Mg^{2+} with the highest field strength improves mechanical properties and that Ba^{2+} having the lowest field strength just like in this study has decreasing effect with the lowest hardness and fracture toughness in the glasses reported.

Brittleness in xBa(40-x)Si fig 6 (d) exhibits a similar trend to the molar volume fig 4 with similar drop at the same compositional ratio 0.33, where brittleness decreased by $1\mu m^{-1/2}$ and then increases linearly with increasing BaO. Brittleness although less often reported is a good parameter to estimate the susceptibility of a material to external mechanical loads; lower brittleness tends to correspond to higher fracture toughness as $B = H/K_{Ic}$. Poisson's ratio in fig 6(e) increases roughly linearly with BaO addition in xBa(40-x)Si glass which can be explained

on the basis of structural depolymerisation induced by the BaO which acts as a modifier (see fig 7) on the degree of polymerisation calculated using the Manara method. Poisson's ratio exhibits inverse correlations with the indentation fracture toughness in xBa(40-x)Si series as presented in fig 6-8

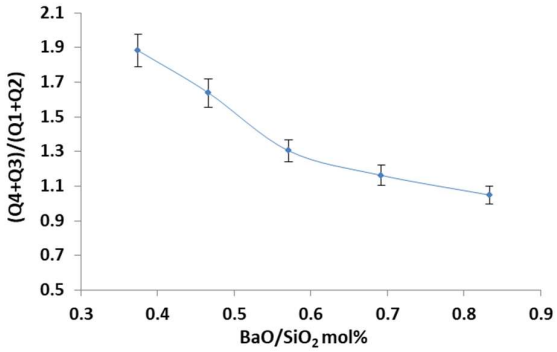

fig 7 Polymerisation index as a function of BaO/SiO_2 content

CONCLUSION

In the xBa(40-x)Si series increasing the alkaline earth content at the expense of the silica content resulted in increased network depolymerisation, it was also found that the moduli and hardness reduced as the network became more depolymerized. Thus BaO act as network modifier and enhance the depolymerisation of the glass network. The fracture toughness measurements show peculiar behavior as it first increases and then decreases with BaO content. Some discrepancies do ocurr between *E* and fracture toughness. Such discrepancies can be explained based on the fact that fracture toughness is not associated only with energy required to break or fracture bonds but also with energy dissipating process such as plastic deformation, crack branching and blunting occuring at the crack tip. For example borate glasses are known to exhibit large inelastic dissipation energies, the magnitude of which depends on the modifier content. Another way to explain difference between *E* and K_{Ic} is to consider the ease of plastic deformation. The density linearly increased with BaO however molar volume exhibited a drop and then rise again. This type of anomalous drop in molar volume have been reported to be associated with the tendency of the network to densify its structure in barium borosilicate glasses at $25<x<48$ mol% of BaO. Although the mechanical properties of sealing glasses are not given a particular targeted value, however, sealing glasses must be able to maintain sufficient mechanical strength to ensure adhesion and gas tightness during sealing and operation at high temperatures and therefore, the values of E, H and indentation fracture toughness in this study are comparable to those reported in the literature. The E moduli of all the glasses are higher than or comparable to most normal borosilicate glasses with 60 to 85GPa ([45], [60]) and the hardness are higher than or comparable to many sealing glasses in the literature [12]. After 50h isothermal heat treatment of xBa(40-x)Si series the glass ceramic contains lanthanum borosilicate phase with PDF card number no (04-010-1343). This particular phase was first reported by [56] and then here we further confirm its presence in the La_2O - B_2O_3- SiO_2 phase diagram.

REFERENCES

1. Zhao, Y. and J. Malzbender, *Elevated temperature effects on the mechanical properties of solid oxide fuel cell sealing materials.* Journal of Power Sources, 2013. **239**(0): p. 500-504.
2. Malzbender, J., Y. Zhao, and T. Beck, *Fracture and creep of glass–ceramic solid oxide fuel cell sealant materials.* Journal of Power Sources, 2014. **246**(0): p. 574-580.
3. Wang, S.-F., et al., *Effect of additives on the thermal properties and sealing characteristic of BaO-Al2O3-B2O3-SiO2 glass-ceramic for solid oxide fuel cell application.* International Journal of Hydrogen Energy, 2009. **34**(19): p. 8235-8244.
4. Ghosh, S., et al., *Microstructure and property evaluation of barium aluminosilicate glass-ceramic sealant for anode-supported solid oxide fuel cell.* Journal of the European Ceramic Society, 2008. **28**: p. 69-76.
5. Mahato, N., et al., *Progress in material selection for solid oxide fuel cell technology: A review.* Progress in Materials Science, 2015. **72**: p. 141-337.
6. Laorodphan, N., et al., *A low silica, barium borate glass-ceramic for use as seals in planar SOFCs.* Journal of Non-Crystalline Solids, 2009. **355**(1): p. 38-44.
7. Ohara, S., et al., *A new sealant material for solid oxide fuel cells using glass-ceramic.* Journal of the Ceramic Society of Japan, 2001. **109**: p. 186-190.
8. Chang, H.-T., C.-K. Lin, and C.-K. Liu, *Effects of crystallization on the high-temperature mechanical properties of a glass sealant for solid oxide fuel cell.* Journal of Power Sources, 2010. **195**: p. 3159-3165.
9. Chang, H.T., et al., *High-temperature mechanical properties of a solid oxide fuel cell glass sealant in sintered forms.* Journal of Power Sources, 2011. **196**(7): p. 3583-3591.
10. Wang, R., et al., *Characteristics of a SiO2-B2O3-Al2O3-BaCO3-PbO2-ZnO glass-ceramic sealant for SOFCs.* Journal of Alloys and Compounds, 2007. **432**: p. 189-193.
11. Coillot, D., et al., *New viscous sealing glasses for electrochemical cells.* International Journal of Hydrogen Energy, 2012. **37**(11): p. 9351-9358.
12. Rodríguez-López, S., et al., *Mechanical properties of solid oxide fuel cell glass-ceramic sealants in the system BaO/SrO-MgO-B2O3-SiO2.* Journal of the European Ceramic Society, 2017. **37**(11): p. 3579-3594.
13. Reis, S.T. and R.K. Brow, *Designing sealing glasses for solid oxide fuel cells.* Journal of Materials Engineering and Performance, 2006. **15**(4): p. 410-413.
14. Sun, T., et al., *Effect of Al 2O 3 content on BaO–Al 2O 3–B 2O 3–SiO 2 glass sealant for solid oxide fuel cell.* Ceramics International, 2010. **36**(2): p. 821-826.
15. Sasmal, N., et al., *Effects of lanthanum oxide on the properties of barium-free alkaline-earth borosilicate sealant glass.* Journal of Non-Crystalline Solids, 2014. **387**: p. 62-70.
16. Larsen, P.H. and P.F. James, *Chemical stability of MgO/CaO/Cr2O3-Al2O3-B2O3-phosphate glasses in solid oxide fuel cell environment.* Journal of Materials Science, 1998. **33**: p. 2499-2507.
17. Kaur, G., O.P. Pandey, and K. Singh, *Self-Healing Behavior of Barium-Lanthanum-Borosilicate Glass and Its Reactivity with Different Electrolytes for SOFC Applications.* International Journal of Applied Ceramic Technology, 2014. **11**(1): p. 136-145.
18. Hsiu-Tao Chang, C.-k.l., Chien-kuo Liu, *High Temperature Mechanical Properties of a Crystallized BaO-B2O3-Al2O3-SiO2 Glass Ceramic for SOFC*, in *ASME 2009*. 2009: Newport Beach, Califonia, U S A.
19. Vepreva, A., et al., *Barium Silicate Glasses and Glass–Ceramic Seals for YSZ-Based Electrochemical Devices.* Ceramics, 2023. **6**(3): p. 1314-1329.
20. Zhao, Y., J. Malzbender, and S.M. Gross, *The effect of room temperature and high temperature exposure on the elastic modulus, hardness and fracture toughness of glass ceramic sealants for solid oxide fuel cells.* Journal of the European Ceramic Society, 2011. **31**(4): p. 541-548.
21. Chang, H.-T., C.-K. Lin, and C.-K. Liu, *High-temperature mechanical properties of a glass sealant for solid oxide fuel cell.* Journal of Power Sources, 2009. **189**(2): p. 1093-1099.

22. Fergus, J.W., *Sealants for solid oxide fuel cells.* Journal of Power Sources, 2005. **147**: p. 46-57.
23. Lessing, P.A., *A review of sealing technologies applicable to solid oxide electrolysis cells.* Journal of Materials Science, 2007. **42**: p. 3465-3476.
24. Mahapatra, M.K. and K. Lu, *Glass-based seals for solid oxide fuel and electrolyzer cells - A review.* Materials Science & Engineering R-Reports, 2010. **67**: p. 65-85.
25. Tulyaganov, D.U., et al., *Aluminosilicate-based sealants for SOFCs and other electrochemical applications - A brief review.* Journal of Power Sources, 2013. **242**: p. 486-502.
26. Larsen, P.H., F.W. Poulsen, and R.W. Berg, *The influence of SiO2 addition to 2MgO–Al2O3–3.3P2O5 glass.* Journal of Non-Crystalline Solids, 1999. **244**(1): p. 16-24.
27. Ghosh, S., et al., *Glass-based Sealants for Application in Planar Solid Oxide Fuel Cell Stack.* Transactions of the Indian Ceramic Society, 2008. **67**(4): p. 161-182.
28. Yang, Z.G., J.W. Stevenson, and K.D. Meinhardt, *Chemical interactions of barium-calcium-aluminosilicate-based sealing glasses with oxidation resistant alloys.* Solid State Ionics, 2003. **160**: p. 213-225.
29. Goel, A., et al., *Effect of BaO on the crystallization kinetics of glasses along the Diopside–Ca-Tschermak join.* Journal of Non-Crystalline Solids, 2009. **355**(3): p. 193-202.
30. Colomban, P., A. Tournie, and L. Bellot-Gurlet, *Raman identification of glassy silicates used in ceramics, glass and jewellery: a tentative differentiation guide.* Journal of Raman Spectroscopy, 2006. **37**(8): p. 841-852.
31. Mysen, B.O., et al., *Curve-fitting of Raman spectra of silicate glasses.* American Mineralogist, 1982. **67**(7-8): p. 686-695.
32. Manara, D., A. Grandjean, and D.R. Neuville, *Advances in understanding the structure of borosilicate glasses: A Raman spectroscopy study.* American Mineralogist, 2009. **94**(5-6): p. 777-784.
33. Smedskjaer, M.M., R.E. Youngman, and J.C. Mauro, *Impact of ZnO on the structure and properties of sodium aluminosilicate glasses: Comparison with alkaline earth oxides.* Journal of Non-Crystalline Solids, 2013. **381**: p. 58-64.
34. Lu, C., et al., *NMR Study on Structural Characteristics of Rare Earth Doped Boro-Alumino-Silicate Glasses.* Journal of Rare Earths, 2006. **24**(4): p. 413-417.
35. Yadav, A.K. and P. Singh, *A review of the structures of oxide glasses by Raman spectroscopy.* Rsc Advances, 2015. **5**(83): p. 67583-67609.
36. Kaur, G., O.P. Pandey, and K. Singh, *Effect of modifiers field strength on optical, structural and mechanical properties of lanthanum borosilicate glasses.* Journal of Non-Crystalline Solids, 2012. **358**: p. 2589-2596.
37. Brow, R.K., D.R. Tallant, and G.L. Turner, *Raman and B-11 nuclear magnetic resonance spectroscopic studies of alkaline-earth lanthanoborate glasses.* Journal of the American Ceramic Society, 1996. **79**(9): p. 2410-2416.
38. Cetinkaya Colak, S., I. Akyuz, and F. Atay, *On the dual role of ZnO in zinc-borate glasses.* Journal of Non-Crystalline Solids, 2016. **432, Part B**: p. 406-412.
39. Kaur, R., S. Singh, and O.P. Pandey, *FTIR structural investigation of gamma irradiated BaO–Na2O–B2O3–SiO2 glasses.* Physica B: Condensed Matter, 2012. **407**(24): p. 4765-4769.
40. Środa, M. and C. Paluszkiewicz, *The structural role of alkaline earth ions in oxyfluoride aluminosilicate glasses—Infrared spectroscopy study.* Vibrational Spectroscopy, 2008. **48**(2): p. 246-250.
41. Parkinson, B.G., et al., *Quantitative measurement of Q3 species in silicate and borosilicate glasses using Raman spectroscopy.* Journal of Non-Crystalline Solids, 2008. **354**(17): p. 1936-1942.
42. Hehlen, B., et al., *Bimodal distribution of Si–O–Si angles in sodo-silicate glasses.* Journal of Non-Crystalline Solids, 2017. **469**: p. 39-44.

43. Kline, J., M. Tangstad, and G. Tranell, *A Raman Spectroscopic Study of the Structural Modifications Associated with the Addition of Calcium Oxide and Boron Oxide to Silica.* Metallurgical and Materials Transactions B, 2015. **46**(1): p. 62-73.
44. Mishra, R.K., et al., *Ionic transport behavior of BaO containing sodium borosilicate glasses.* Journal of Hazardous Materials, 2009. **161**(2): p. 1450-1453.
45. Ghosh, S., et al., *Effect of BaO addition on magnesium lanthanum alumino borosilicate-based glass-ceramic sealant for anode-supported solid oxide fuel cell.* International Journal of Hydrogen Energy, 2010. **35**(1): p. 272-283.
46. Lahl, N., et al., *Crystallisation kinetics in AO-Al2O3-SiO2-B2O3 glasses (A = Ba, Ca, Mg).* Journal of Materials Science, 2000. **35**: p. 3089-3096.
47. Staff, M.T., et al., *Fabrication of a Glass-Ceramic-to-Metal Seal Between Ti–6Al–4V and a Strontium Boroaluminate Glass.* International Journal of Applied Ceramic Technology, 2016. **13**(5): p. 956-965.
48. Qi, S., et al., *High-temperature glassy-ceramic sealants SiO2—Al2O3—BaO—MgO and SiO2—Al2O3—ZrO2—CaO—Na2O for solid oxide electrochemical devices.* Transactions of Nonferrous Metals Society of China, 2016. **26**(11): p. 2916-2924.
49. Hao, J., et al., *Structure and high temperature physical properties of glass seal materials in solid oxide electrolysis cell.* Journal of Power Sources, 2012. **214**: p. 75-83.
50. Deshpande, A.V. and V.K. Deshpande, *Correlation of glass transition temperature and density with electrical conductivity of lithium sulfoborosilicate glasses.* Solid State Ionics, 2006. **177**(26–32): p. 2747-2751.
51. Monteiro, R., et al., *SINTERING, CRYSTALLISATION, AND DIELECTRIC BEHAVIOUR OF BARIUM ZINC BOROSILICATE GLASSES - EFFECT OF BARIUM OXIDE SUBSTITUTION FOR ZINC OXIDE.* Journal of the American Ceramic Society, 2012. **95**(10): p. 3144-3150.
52. Bootjomchai, C., et al., *Elastic moduli of borosilicate glasses doped with heavy metal oxides.* Journal of Non-Crystalline Solids, 2014. **388**: p. 37-45.
53. Abd El-Moneim, A., I.M. Youssof, and L. Abd El-Latif, *Structural role of RO and Al2O3 in borate glasses using an ultrasonic technique.* Acta Materialia, 2006. **54**(14): p. 3811-3819.
54. Bourgel, C., et al., *Molar volume minimum and adaptative rigid networks in relationship with the intermediate phase in glasses.* Physical Review B - Condensed Matter and Materials Physics, 2009. **79**(2).
55. Trégouët, H., et al., *Exploration of glass domain in the SiO2-B2O3-La2O3 system.* Journal of Non-Crystalline Solids, 2017.
56. Shvanskii, E.V., et al., *Crystallization and structural characteristics of new borosilicates.* Journal of Solid State Chemistry, 2000. **154**(1): p. 312-316.
57. Nicoleau, E., et al., *Rare-earth silicate crystallization in borosilicate glasses: Effect on structural and chemical durability properties.* Journal of Non-Crystalline Solids, 2016. **438**: p. 37-48.
58. Hand, R.J. and D.R. Tadjiev, *Mechanical properties of silicate glasses as a function of composition.* Journal of Non-Crystalline Solids, 2010. **356**(44–49): p. 2417-2423.
59. Yoshida, S., et al., *Scratch Resistance of Sodium Borosilicate Glass.* Journal of the Ceramic Society of Japan, 2001. **109**(1270): p. 511-515.
60. Vullo, P. and M.J. Davis, *Comparative study of micro-indentation and Chevron notch fracture toughness measurements of silicate and phosphate glasses.* Journal of Non-Crystalline Solids, 2004. **349**: p. 180-184.